Fuzzy Gain-Scheduled Missile Autopilot Design using Evolutionary Algorithms

T. Sreenuch, A. Tsourdos, E. J. Hughes and B. A. White
Department of Aerospace, Power and Sensors, Cranfield University - RMCS
Shrivenham, Swindon, SN6 8LA, UK

Abstract— **The paper presents the lateral acceleration control design of a missile model using the evolution strategy. The non-linear fixed-structure-like controller is represented by the singleton fuzzy model. This allows a variation of shapes of the gain functions to be explored, and subsequent modification is fairly easy. Instead of finding an optimal decomposition of the fuzzy controller, a set of fuzzy rule is unconventionally optimized for the overall gain surfaces that guarantee acceptable performances for the closed-loop system over the whole operating envelope. The simulation results show that the designed fuzzy gain-scheduled controller is a robust tracking controller for all perturbation vertices.**

I. Introduction

This paper looks at the application of fuzzy modeling to a robust autopilot design. The aim is to synthesize the non-linear fixed-structure-like controller by shaping the system's open- and closed-loop frequency responses results in the closed-loop responses are within the tracking bounds without violating the actuator constraints. Finding a feasible non-linear controller that meet the desired specifications can be very difficult. By formulating the former to an optimization problem, the specific solutions on the Pareto front can be identified using the evolution strategy (ES) as described in [1]. In this study, the optimized surfaces of the controller's poles, zeros and gains are conveniently be formulated in term of piecewise-linear like fuzzy systems. This allows a variation of shapes of the gain functions to be explored, and subsequent modification is fairly easy. Instead of finding an optimal decomposition of the fuzzy controller, a set of fuzzy rule is unconventionally optimized for the overall gain surfaces that guarantee acceptable performances for the closed-loop system over the whole operating envelope.

II. Missile Model and Autopilot Requirements

A. Non-Linear Model

The missile model used in this study is taken from Horton's MSc thesis [2]. It describes a 5 degree-of-freedom (DOF) model in parametric format with cross-coupling and non-linear behaviour. In this study, the airframe is roll stabilized. The problem of controlling a missile in roll are relatively minor and the roll stabilized airframe imparts little cross-coupling between axes. Therefore, the subject of this study will look at the reduced problem of a controller for the uncoupled lateral motion (on the xy plane in Fig. 1). The airframe is roll stabilised ($\lambda = 45°$), and no coupling

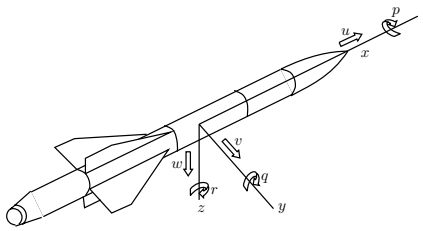

Fig. 1. Airframe axes and nomenclature.

is assumed between pitch and yaw channels. With these assumptions, the equations of motion are given by

$$\begin{aligned} \dot{v} &= y_v v + y_\zeta \zeta - Ur, \\ &= \frac{1}{2m}\rho V S(C_{y_v} v + V C_{y_\zeta}\zeta) - Ur, \quad (1) \\ \dot{r} &= n_v v + n_r r + n_\zeta \zeta, \\ &= \frac{1}{2I_z}\rho V S d(C_{n_v} v + \frac{1}{2} d C_{n_r} r + V C_{n_\zeta}\zeta), \quad (2) \\ a_y &= \dot{v} + Ur, \quad (3) \end{aligned}$$

where v the lateral velocity, r the body rate, ζ the rudder fin deflections, U the forward velocity and a_y the lateral acceleration at the centre of gravity $c.g.$ are defined in figure 1. y_v, y_ζ are semi-non-dimensional force derivatives due to lateral velocity and fin deflection. n_v, n_r, n_ζ are semi-non-dimensional force derivatives due to lateral velocity, body rate and fin deflection. The aerodynamic derivative C_{y_v}, C_{y_ζ}, C_{n_v}, C_{n_r} and C_{n_ζ} are the function of Mach number M and incidence angle σ ($\approx v/U$ for $U \gg v$). They are evaluated by interpolating the discrete data points obtained from the wind tunnel experiments. These interpolated formulas and other relevant physical parameters are summarised in table I and II.

B. Airframe Transfer Function

Applying the Laplace transform to the state and output equation (1)-(3) gives body rate and acceleration transfer functions of

$$P_{r_\zeta}(s) = \frac{n_\zeta s - (n_\zeta y_v - n_v y_\zeta)}{s^2 - (y_v + n_r)s + (U n_v + y_v n_r)}, \quad (4)$$

$$P_{a_{y_\zeta}}(s) = \frac{y_\zeta s^2 - y_\zeta n_r s - U(n_\zeta y_v - n_v y_\zeta)}{s^2 - (y_v + n_r)s + (U n_v + y_v n_r)}. \quad (5)$$

The weathercock mode is given by the denominator of equation (4) and (5) and, with typical semi-non-dimensional

Symbol	Meaning	Value
a	Speed of sound	340 m/s
ρ	Air density	1.23 kg/m^3
d	Reference diameter	0.2 m
S	Reference area	0.0314 m^2
m	Mass	150 kg full 100 kg all burnt
I_z	Lateral inertia	75 kg $\cdot$ m^2 full 60 kg $\cdot$ m^2 all burnt
x_{cg}	Centre of gravity	$1.3 + m/50$
x_{cp}	Centre of pressure	$1.3 + 0.1M + 0.3\|\sigma\|$
x_f	Fin centre of pressure	2.6 m
x_m	Static margin	$x_{cg} - x_{cp}$
x_f	Fin moment arm	$x_{cg} - x_f$

TABLE I

PHYSICAL PARAMETERS.

Corresponding force or moment	Aerodynamic derivative	Interpolated formula
Side force	C_{y_v}	$-26 + 1.5M - 60\|\sigma\|$
	C_{y_ζ}	$10 - 1.4M + 1.5\|\sigma\|$
Yawing moment	C_{n_v}	$s_m C_{y_v}$, where $s_m = x_m/d$
	C_{n_r}	$-500 - 30M + 200\|\sigma\|$
	C_{n_ζ}	$s_f C_{y_\zeta}$, where $s_f = x_f/d$

TABLE II

AERODYNAMIC DERIVATIVES.

derivatives, shows the polynomial to be lightly damped with a weathercock frequency that is dominated by the term Un_v.

C. Autopilot Configuration

The lateral autopilot configuration used in this paper is shown in Fig. 2, where $F(s) = 98700/(s^2+445s+98700)$

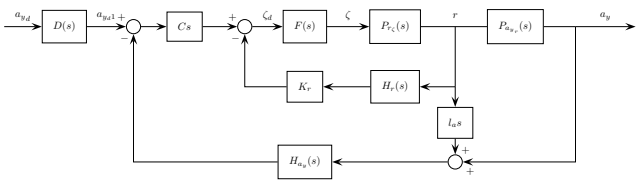

Fig. 2. 2 DOF autopilot configuration.

is the fin servo dynamics with maximum fin angle of ± 0.3 rad and rate of ± 15 rad/s, $H_r(s) = 253000/(s^2 + 710s + 253000)$ is the rate gyro dynamics, and $H_{a_y}(s) = 394800/(s^2 + 890s + 394800)$ is the lateral accelerometer dynamics. The accelerometer is placed at a position displaced from the missile's c.g., 0.7 m aft the nose. This produces measured acceleration a_{y_m} that contains component of angular acceleration of

$$a_{y_m} = a_y + l_a \dot{r}, \tag{6}$$

where l_a is the accelerometer moment arm from the c.g. The control structure incorporates a lag-lead in the error limb and is closed around acceleration feedback with body rate feedback used to improve the closed-loop stability. With an additional pre-filter, there is no direct relationship the stability margins of the feedback system and its time-domain response (in practice, it is very important to have it). The autopilot is designed by setting K_r the gyro gain, $C(s)$ the lag-lead compensator and $D(s)$ the pre-filter to have acceptable closed-loop frequency-domain tracking performances.

Define $P_{a_{y_r}}(s) = a_y(s)/r(s)$, $G(s) = -C(s)F(s)/(1 - K_r F(s) P_{r_\zeta}(s) H_r(s))$, and $H(s) = (l_a s P^{-1}_{a_{y_r}}(s) + 1) H_{a_y}(s)$. The following key transfer functions will be used throughout:

1. The open loop transfer function

$$L(s) = G(s)P(s)H(s). \tag{7}$$

2. The sensitivity function

$$S(s) = \frac{1}{1 + L(s)}. \tag{8}$$

3. The tracking transfer function

$$T(s) = D(s)G(s)P_{a_{y_\zeta}}(s)S(s). \tag{9}$$

4. The control sensitivity function

$$Q(s) = D(s)G(s)S(s). \tag{10}$$

D. Closed-Loop Performance Specifications

The autopilot is required to track a lateral acceleration demand a_{y_d} over the whole flight envelope, where $|a_{y_d}| \leq 500$ m/s^2 is constrained by limitations on the airframes structural integrity. It must be as robust to the variation in fuel state and airframe parameter estimation errors. It should also be stable in the presence of fin servo non-linearities. A list of performance specifications for a step input is given in the mixed time- and frequency-domain using familiar figures as follows: [2]

1. Bandwidth $\omega_{-3\text{ dB}} > 40$ rad/s (1.5 times the weathercock natural frequency),
2. Settling time variation $|\delta_{t_s}| \leq 0.05$ s,
3. Steady state error $e_{ss} \leq 10$ %,
3. Overshoot $M_p \leq 10\%$,
4. Gain margin $GM \geq 9$ dB, Phase margin $PM \geq 40^\circ$.

III. DESIGN OF LATERAL MISSILE AUTOPILOT

A. Uncertainty Model

As is shown in equation (4) and (5), the semi-non-dimensional aerodynamic derivatives contribute to the variation of coefficients of transfer functions, which lead to the multiple linear models when describing the different operating conditions.

In this missile study, the solid propellant motor is capable of a boost-coast thrust profile. The thrust is modeled by a specific impulse of duration 3.5 s in which the increment velocity during boost is seen to range form Mach 1.8 to 3.9. The missile mass and inertia are modeled as linear functions of the propellent burn. The mass variation as a function of Mach number is shown in Fig. 3.

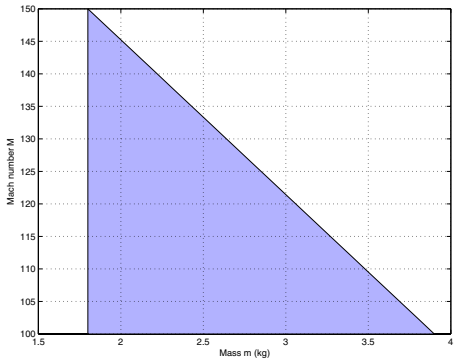

Fig. 3. Mass variation.

The aerodynamic derivatives can be evaluated with good accuracy from the wind tunnel experiment. However, the resulting evaluations can only be regarded as estimates of the exact values. In this missile study, the degree of confidence associated with the derivative estimates is assumed to be $\pm 5\%$, i.e. $-0.05 \leq \Delta_{x_{cp}}, \Delta_{C_{y_v}}, \Delta_{C_{y_\zeta}}, \Delta_{C_{n_r}} \leq 0.05$.

B. Measures of Performance

1) Asymptotic Stability: The stability of the closed-loop system can graphically be checked using the Nyquist plot or Nichols chart. However, it is numericly difficult. In this paper, the stability of the closed-loop system is simply determined by solving the roots of the characteristic polynomial. The function

$$C_0 = \begin{cases} 0 & \text{if } S(s) \text{ is asymptotically stable,} \\ 1 & \text{otherwise,} \end{cases} \tag{11}$$

To ensure internal stability, we must guarantee not only stability of $S(s)$ but also that there is no RHP pole-zero cancellation when $L(s)$ is formed. One way to achieve this is it is desired that minimum phase and stable controller $C(s)$ is designed.

2) Gain and Phase Margins: A look at the inverted Nichols chart in Fig. 4 qualitatively reveals that gain and phase margins decrease as the values of the contours of constant $|S(j\omega)|$ increases. For instance, if $|S(j\omega)| \leq 3$ dB,

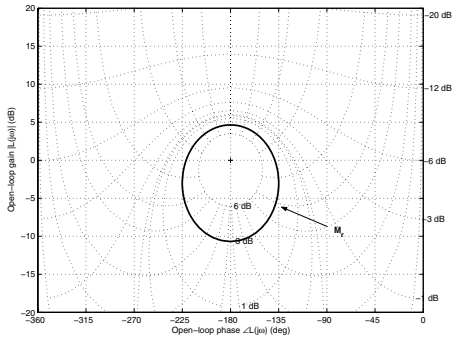

Fig. 4. Inverted Nichols chart.

then $GM > 10$ dB and $PM > 40^\circ$ are guaranteed. [3]

Adopting these relationships, the gain-phase margin based cost function can be given by

$$O^{(1)} = \max_{\omega} \frac{|S(j\omega)| - M_0}{M_r - M_0}, \tag{12}$$

where $M_0 = -6$ dB, and M_r is the admissible resonant peak of the sensitivity function $S(j\omega)$.

3) Tracking Error: The system's tracking performance specifications are based upon satisfying all of the frequency forcing functions $|B_U(j\omega)|$ and $|B_L(j\omega)|$ shown in Fig. 5a. They represent the upper and lower bounds of tracking

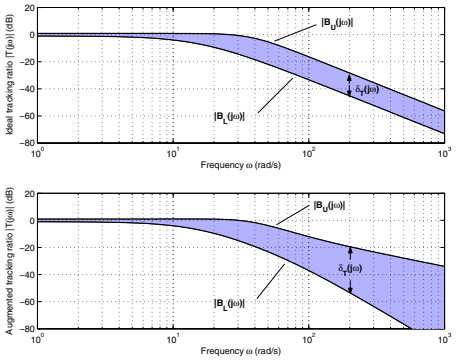

Fig. 5. Ideal and augmented tracking models.

performance specifications whom an acceptable response $|T(j\omega)|$ must lie within. However, the difference between $|B_U(j\omega)|$ and $|B_L(j\omega)|$ is required to increase with increasing frequency. This can be achieved by augmenting $B_U(s)$ with a zero as close to the origin as possible without significantly affecting the time response (see Fig. 5b). The spread can be further increased by similarly augmenting $B_L(s)$ with a real negative pole. [4]

Following this design concept, the tracking boundaries based cost function can be defined by

$$O^{(2)} = \max_{\omega} \left\{ \frac{|T(j\omega)| - |T_0(j\omega)|}{|B_U(j\omega)| - |T_0(j\omega)|}, \frac{|T_0(j\omega)| - |T(j\omega)|}{|T_0(j\omega)| - |B_L(j\omega)|} \right\}, \tag{13}$$

where $|T_0(j\omega)|$ is the nominal tracking model.

4) Actuator Rate Limit: Another issue that must be addressed in the autopilot design is the fin time responses that contain a saturation in both rate and deflection. They can be examined in relation to the maximum lateral acceleration that can be commanded at each flight condition throughout the operating envelope. In this missile study, the fin rate limit is only considered. The fin deflection is unlikely to saturate in this case. However, there are no exact analytical means for translating the magnitude response of a transfer function into its step time response. Thus, an estimate of the resulting fin rate has to inevitably be obtained by simulating the impulse response of $Q(s)$.

Then, the fin rate limit based cost function can be given by

$$O^{(3)} = \sup_{0 \le t} \frac{\dot{\zeta}(t)}{R}, \tag{14}$$

where R is the allowed fin deflection rate for a unit-step command.

IV. Fuzzy Gain-Scheduled Controller

A. Fuzzy System as Piecewise-Linear Interpolation

It remains to determine a scheduling algorithm for selecting the local controller to be applied. The operating regimes can conveniently be described as fuzzy sets and fuzzy inferences by which the soft transition (i.e. a kind of interpolation) between the operating regimes can be handled in a natural way. This representation is appealing since many systems change their dynamics smoothly as a function of the operating point.

In what follows, we consider a fuzzy controller described by a set of rules on the form

$$\begin{aligned} R_i \ &: \text{IF } x^{(1)} \text{ is } A_{i1} \text{ AND} \ldots \text{AND } x^{(m)} \text{ is } A_{im} \\ &\text{THEN } y^{(1)} = b_{i1} \text{ AND} \ldots \text{AND } y^{(n)} = b_{in}, \end{aligned} \tag{15}$$

where $i = 1, \ldots, N$, N is the number rules, $x^{(i)}$ are the antecedent variables represent the input of the fuzzy system, A_{ij} are the fuzzy sets and b_{ij} are the consequent values represent the output of the fuzzy system. This model is called the singleton model. Descriptively, each rule premise defines an operating regime and the associated rule consequent specifies the local controller valid within this region. By the appropriate restrictions of the fuzzy inference parameters, the controller's outputs inferred from the rules (5.1) can be written as

$$y_i = \frac{\sum_{j=1}^{N} \beta_j(\vec{x}) b_{ij}}{\sum_{j=1}^{N} \beta_{ij}(\vec{x})}, \tag{16}$$

where $\beta_i = \prod_{j=1}^{m} \mu_{ij}(\vec{x})$ and $0 \le \mu_{ij}(\vec{x}) \le 1$ is the membership function.

In general, the characteristics of the fuzzy controller (15) are non-linear. The form of developed non-linearity relies upon the analytical form of the membership functions A_{ij}. Quite often these are defined by means of the trapezoidal or triangular membership functions that are pairwise overlapping and the membership degrees sum up to one for each domain element. Under these additional assumptions, we end up dealing with the piecewise linear input-output relationship. A univariate example is shown in Fig. 6. The knots of the piecewise linear characteristic of the controller are at the modal values of the A_j's. The slope of the control relationship is easily computed as the ratio $(b_j - b_{j-1})/(a_i - a_{j-1})$. Note that, by adjusting the position of the linguistic terms or/and modifying the local control values, one can easily effect the gain of the controller that applies to this specific region.

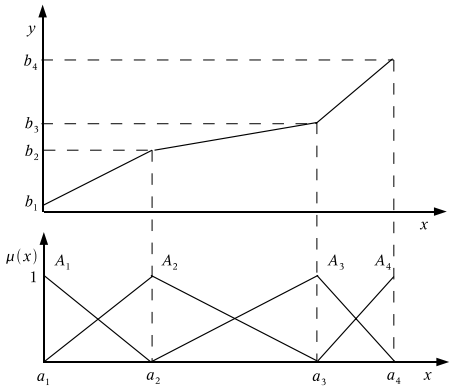

Fig. 6. Piecewise linear characteristics of the fuzzy controller.

B. Parameter Characterization and Coding

The autopilot is designed by setting K_r, $C(s)$ and $D(s)$ to meet the frequency-domain requirements. In this study, K_r, $C(s)$ and $D(s)$ are parametrized in terms their poles, zeros and gain. Suppose the control structure is prespecified, e.g.

$$K_r,\ C(s) = K_p \frac{(s+z_1)(s+z_2)}{(s+p_1)(s+p_2)} \text{ and } D(s) = \frac{K_d}{s+p_d}. \tag{17}$$

Recall that an operating point is characterized by the Mach number and incidence. From Fig. 7, the input ranges are 1.8 to 3.9 for the Mach number and 0 to 0.327 rads for the incidence. With n member functions per input, then there will be n^2 possible rules. The output values for each each rule are simply the constant controller's poles, zeros and gains. Hence, the fuzzy rule R_i of the system in question can be given by

$$\begin{aligned} R_j \ &: \text{IF } M \text{ is } A_j \text{ AND } \sigma \text{ is } B_j \\ &\text{THEN } K_r = K_{r_j} \text{ AND} \ldots \text{AND } p_d = p_{d_j}, \end{aligned} \tag{18}$$

where $j = 1, \ldots, n^2$ and $A_j = [M_j^-, M_j^+]$ and $B_j = [\sigma_j^-, \sigma_j^+]$ define the corresponding jth operating region.

In this case, the optimized parameters are the values characterizing the membership functions of the antecedents and the numerical values of the outputs. Thus, a multi-parameter concatenation

$$\vec{x} = [a_2, \ldots, a_{n-1}, b_2, \ldots, b_{n-1}, \bar{K}_{r_1}, \ldots, \bar{p}_{d_{n^2}}], \tag{19}$$

where a_j and b_j locate the peaks of the membership functions (see Fig. 6), forms a variable vector for the ES [5].

C. Fuzzy Rules Tuning

In the simplest case, we start with a case of 2 membership functions for each of the two inputs. The (100+100)-ES was applied to tune the consequent values for each fuzzy rule. The performance of the fuzzy controller was tested over a grid of operating points shown in Fig. 7, where the number of incidence conditions required are rounded to the nearest integers.

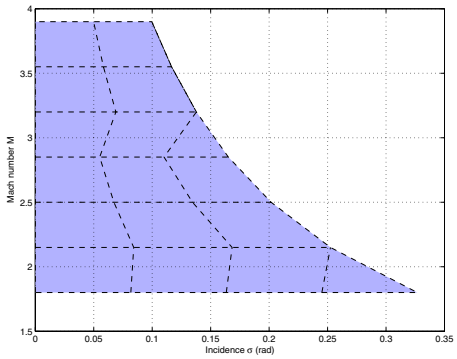

Fig. 7. A grid of operating points.

Initial finding shows that p_2 are in fact outside the influence frequency range. To keep the controller proper, these far-off poles can be fixed, says, at $\omega = 10000$ rad/s, which are sufficiently distanced from the considered frequency range. With this lag-lead structure, there is now a total of 28 optimized parameters.

It has to be noted that robustness analysis of an uncertain system can be computationally very expensive. In fact, using the vertex points is enough in robust controller design for most practical systems. To reduce the computational cost, the similar optimization process as described in [6] is followed, where addition vertices are added in each loop until an optimal solution satisfies the search critieria.

The proposed configuration was optimized, and its cumulative trade-off graph is shown in Fig. 8. The optimization time required was about 5 hours.

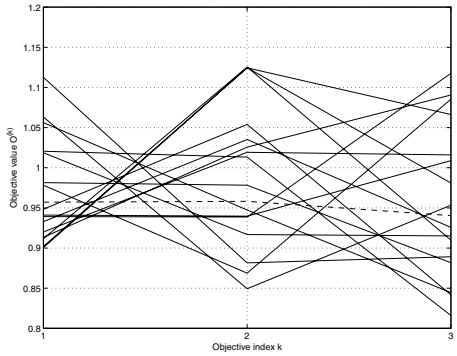

Fig. 8. Cumulative trade-off graph of the fuzzy controller.

D. Evaluation of the Design Solution

Suppose the unity-weight min-max solution (dashed line in Fig. 8) is preferred. The associated fuzzy consequences are shown in table III. The templates of $L(j\omega)$ are compute using the edges of the parameter box. Fig. 9 shows the Nichols plot of the resultant templates. $L(j\omega)$ under the prescribed plant set does not encircle point in case of stable open-loop and counter-clockwise encircles if $L(s)$ is unstable. Moreover, it lies outside the allowed contour of

Knot location	Consequent parameters
(1.8,0)	$K_r = 0.11,$ $C(s) = 0.047\dfrac{(s+11.496)(s+440.734)}{(s+2.027)(s+10000)},$ $D(s) = \dfrac{11.45}{s+11.315}.$
(1.8,0.327)	$K_r = 0.0964,$ $C(s) = 0.034\dfrac{(s+14.073)(s+346.444)}{(s+1.023)(s+10000)},$ $D(s) = \dfrac{13.181}{s+12.178}.$
(3.9,0)	$K_r = 0.037,$ $C(s) = 0.023\dfrac{(s+48.086)(s+48.069)}{(s+1.523)(s+10000)},$ $D(s) = \dfrac{31.788}{s+29.932}.$
(3.9,0.327)	$K_r = 0.045,$ $C(s) = 0.0016\dfrac{(s+33.714)(s+227.601)}{(s+1.954)(s+10000)},$ $D(s) = \dfrac{9.45}{s+8.876}.$

TABLE III
FUZZY RULES' CONSEQUENCES.

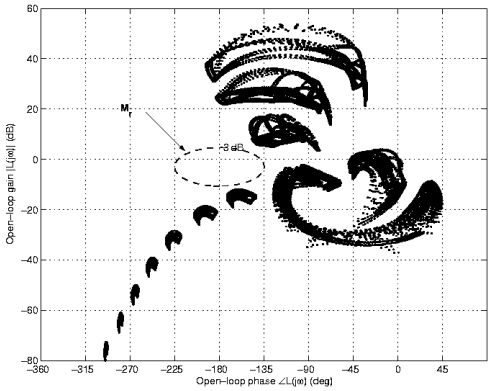

Fig. 9. Nichols template of $L(j\omega)$.

constant $|S(j\omega)|$. This suggests that the closed-loop is stable with adequate gain and phase margins. A further analysis, using the recursive grid method to obtain bode envelope for the closed-loop transfer function, dashed line in Fig. 10, reveals that this controller is indeed robust performance for all possible perturbations. The selected vertices of $|Q(j\omega)|$ are plotted in Fig. 11. The influence of the non-minimum phase zero on $|Q(j\omega)|$ (occurrence of the side-lope) is clearly visible.

The designed gain-scheduled controller satisfies the desired frequency domain performance specifications for all possible perturbations. The time responses of the gain-scheduled controller is shown in Fig. 12. The simulation results show that the controller is a robust tracking gain-

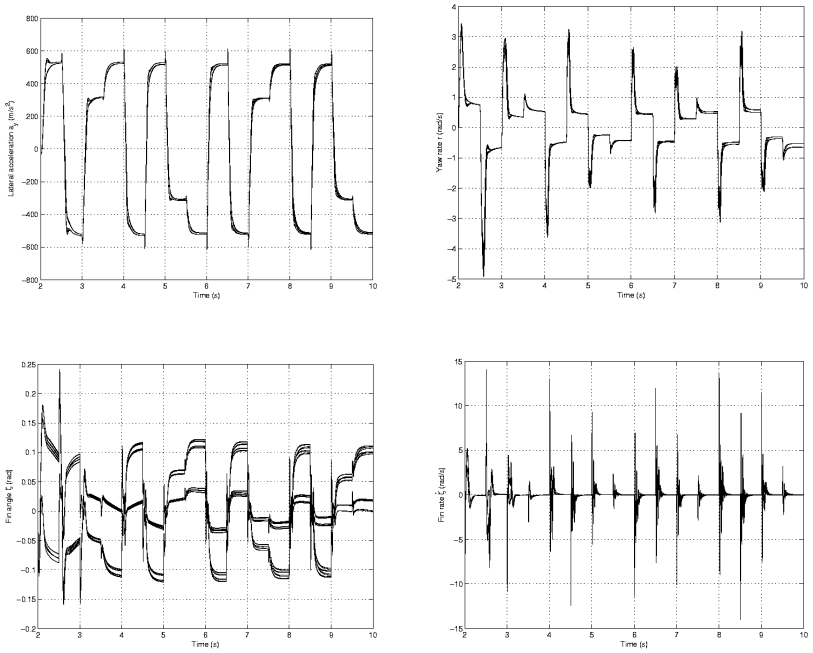

Fig. 12. Lateral acceleration sequence step response of the perturbation vertex systems.

scheduled controller, at least for all the perturbation vertices. There is no sign of rate saturation in the fin responses.

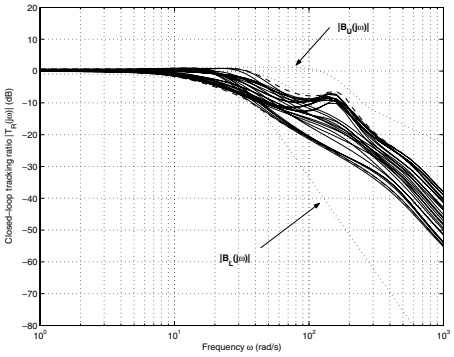

Fig. 10. Bode envelope of $|T(j\omega)|$.

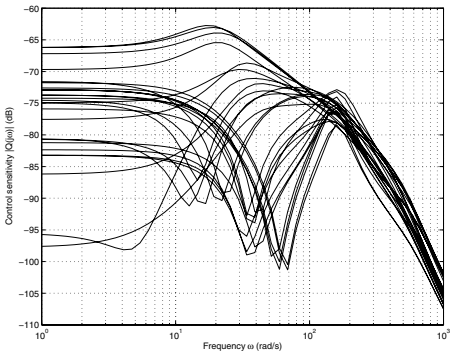

Fig. 11. Bode plots of $|Q(j\omega)|$.

V. Conclusion

This paper looks at the application of fuzzy modeling to a robust autopilot design. The optimized surfaces of the non-linear fixed-structure-like controller's poles, zeros and gains are conveniently be formulated in term of piecewise-linear-like fuzzy systems. This allows a variation of shapes of the gain functions to be explored, and subsequent modification is fairly easy. Unlike conventional TS fuzzy controller, the closed-loop performances are guaranteed for the resulting optimized gain-scheduled controller. The method however suffers from the image of computational inefficiency as the optimized parameters are a square factor of the number of member functions per input.

References

[1] K. Deb. *Multi-Objective Optimization using Evolutionary Algorithms*. Wiley-Interscience Series in Systems and Optimization. John Wiley and Sons, Chichester, 2001.

[2] M. P. Horton. A study of autopilots for the adaptive control of tactical guided missiles. Master's thesis, University of Bath, Bath, UK, 1992.

[3] M. Sidi. *Design of Robust Control Systems: From Classical to Modern Practical Approaches*. Krieger, Malabar, Florida, 2001.

[4] C. H. Houpis and S. J. Rasmussen. *Quantitative Feedback Theory: Fundamentals and Applications*. Control Engineering. Marcel Dekker, New York, 1999.

[5] L. Fortuna, G. Rizzotto, M. Lavorgna, G. Nunnari, M. G. Xibilia, and R. Caponetto. *Soft Computing: New Trends and Applications*. Springer, 2001.

[6] M. T. Söylemez. *Pole Assignment for Uncertain Systems*. UMIST Control Systems Centre Series. Research Studies Press, Hertfordshire, 1999.